Electronic structure of the Cu_3O_4 plane of $Ba_2Cu_3O_4Cl_2$: Experiment and theory

H. C. Schmelz, M. S. Golden, S. Haffner, M. Knupfer, G. Krabbes, and J. Fink
Institute for Solid State and Materials Research (IFW) Dresden, P. O. Box 270016, D-01171 Dresden, Germany

H. Rosner, R. Hayn, and H. Eschrig
Max-Planck-Arbeitsgruppe Elektronensysteme, TU Dresden, D-01062 Dresden, Germany

A. Müller
Institut für Physik, Humboldt Universität zu Berlin, Invalidenstrasse 110, D-10115 Berlin, Germany

Ch. Jung and G. Reichardt
BESSY GmbH, Lentzeallee 100, D-14195 Berlin, Germany

(Received 18 November 1997)

We present a detailed joint experimental and theoretical investigation of the valence band electronic structure of single crystals of the model cuprate $Ba_2Cu_3O_4Cl_2$. This oxychloride system possesses a Cu_3O_4 plane which can be regarded as a superposition of two subsystems: a Cu_AO_2 cuprate plane and an extra Cu_B site, and thus represents an ideal trial system for assessing the impact of deviations from the CuO_2 plane stoichiometry upon the electronic structure in cuprate materials. From polarization-dependent, **k**-resolved photoemission measurements the dispersion relations and symmetry of a number of the observed valence band features are determined and compared with the results of band structure calculations carried out within the LSDA+U formalism, which include a detailed analysis of the character and symmetry of the individual bands. Upon electron removal, the extra copper site makes its presence felt via the formation of a second Zhang-Rice singlet located on the Cu_B subsystem, in addition to that originating from the Cu_AO_2 subsystem. The main valence band edge at ~ 2 eV binding energy is shown to be mainly due to bands involving combinations of O $2p_{x,y}$ orbitals, some of which exhibit essentially pure O $2p$ character. These low-lying oxygen bands are different in origin from the nonmixing O $2p$ states observed, for example, at (π,π) in $Sr_2CuO_2Cl_2$, as the orbital combination responsible for the latter is involved in $Ba_2Cu_3O_4Cl_2$ in the formation of the Zhang-Rice singlet state on the Cu_B sublattice. [S0163-1829(98)00717-6]

I. INTRODUCTION

Despite the tremendous experimental and theoretical effort which has been dedicated to the study of the high-temperature superconductors (HTSC's) over the last ten years,[1–3] there is still no microscopic theory explaining the high transition temperatures of these materials. One approach is to study model cuprates, in which the properties of an isolated copper oxide plane can be investigated both experimentally and theoretically. The strategy is such that the understanding gained from the study of these materials can be transferred to the more complex real high-T_c materials.

One such class of model cuprates are the oxychlorides which include the compounds $Sr_2CuO_2Cl_2$ and $Ba_2Cu_3O_4Cl_2$. The former possesses single CuO_2 planes separated by Sr-Cl block layers, and has been the subject of much attention as a near ideal representative of a 2D spin-$\frac{1}{2}$ Heisenberg antiferromagnet.[4] $Ba_2Cu_3O_4Cl_2$ shares the same tetragonal symmetry, but has Cu_3O_4 planes whose electronic states are highly two dimensional as a consequence of the lack of apical atoms directly above the Cu sites.[5] In the Cu_3O_4 plane of $Ba_2Cu_3O_4Cl_2$, two thirds of the copper atoms occupy the usual cuprate site, denoted Cu_A, with the remaining third of the copper atoms being located at an additional site, denoted Cu_B (see Fig. 1). This geometry can be thought of as two interpenetrating sublattices: a cupratelike Cu_AO_2 sublattice and a sublattice based upon the additional Cu_B atoms. Both of these two sublattices are 2D spin-$\frac{1}{2}$ quantum antiferromagnets,[6] although they have widely differing Néel temperatures. First, the Cu_AO_2 sublattice orders at 330 K,[7] a T_N^A typical for cuprates with strong superexchange coupling via 180° Cu_A-O-Cu_A interactions. Second, the Cu_B sublattice orders at a much lower T_N^B of 31 K.[7] The Cu_B spins are frustrated with respect to the Cu_A spin system, and can only couple with it via 90° Cu_B-O-Cu_A interactions (thus involv-

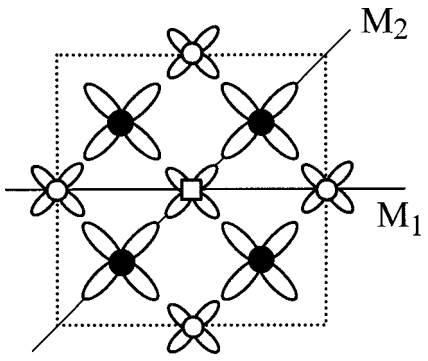

FIG. 1. A schematic representation of a unit cell the Cu_3O_4-plane in $Ba_2Cu_3O_4Cl_2$. ○ : cupratelike Cu_A; □ : additional Cu_B; ● : oxygen. M_1 and M_2 represent the two mirror planes (see text). The O $2p_{x,y}$ and Cu $3d_{x^2-y^2}$ atomic orbitals are also shown.

ing orthogonal O $2p$ orbitals). Thus measurements at or near room temperature probe a system with an antiferromagnetically ordered Cu_AO_2 and a paramagnetic Cu_B sublattice. In terms of the local CuO_4 geometry, however, the two copper sites are identical and both are formally in the Cu^{2+} valence state.

Angle-resolved photoemission spectroscopy (ARPES) is a powerful spectroscopic tool in the study of the electronic structure of solids. Despite the fact that the model cuprates are undoped, information relevant to the hole states formed upon chemical doping can be obtained via ARPES measurements, as photoemission necessarily involves the creation of a hole in the electron system under investigation. Such measurements are thus equivalent to the examination of the electronic structure of the system in the limit of extremely low chemical doping. Therefore ARPES investigations of $Ba_2Cu_3O_4Cl_2$ represent an ideal method with which to assess the impact of the different Cu-O plane geometry upon the electronic structure of a cuprate. This has been demonstrated recently in a study of the dispersion of a hole in the highest occupied valence band of $Ba_2Cu_3O_4Cl_2$.[8] In this paper we compare further polarization-dependent ARPES experiments on $Ba_2Cu_3O_4Cl_2$ with the results of band structure calculations carried out within the local spin-density approximation in which the effect of strong electron correlation on the quasiparticle self-energy has been taken approximately treated (LSDA+U).

II. METHODS

Single crystals of $Ba_2Cu_3O_4Cl_2$ were grown from the melt. Clean surfaces were prepared for photoemission by cleaving in an ultrahigh vacuum, whereby the quality and orientation of the resulting surface were checked *in situ* using low-energy electron diffraction. The crystals cleave parallel to the Cu_3O_4 planes. During the experiment the sample was held at 360 K, which was found to minimize charging effects and prolong the lifetime of the surface. Spectra were also recorded at 295 K (i.e., below T_N^A), and were identical within the experimental error to those presented here.[9] The base pressure in the ARPES chamber was below 2×10^{-10} mbar and the spectra did not show any changes under these conditions for at least two days. All spectra were recorded for a number of cleavages. Monochromatized synchrotron radiation with an energy of 35 eV from the crossed-undulator beamline U2-FSGM,[10] at the BESSY electron storage ring facility in Berlin was used as the photon source. The angular resolution of the electron energy analyzer, which is situated at an angle of 60° with respect to the incoming synchrotron radiation, was set to $\pm1°$ (corresponding to a **k** resolution of 0.16 π/a) and the overall energy resolution of the system was chosen to be 160 meV. Due to charging effects, the absolute binding energy (BE) scale was determined in two steps: first a self-consistent relative BE for the ARPES series was obtained using the spectra recorded for the energy region of the Ba $5p$ doublet (BE 12–20 eV) for each emission angle directly after the respective valence band measurement. An absolute BE scale was then derived by extrapolating the BE of the Ba $5p$ doublet to zero incident photon intensity and correcting the ARPES valence band spectra correspondingly. However, this procedure necessarily introduces an error in the absolute BE's which we estimate to be ±0.1 eV. The spectra are normalized to have equal maximal intensity in the energy region shown.

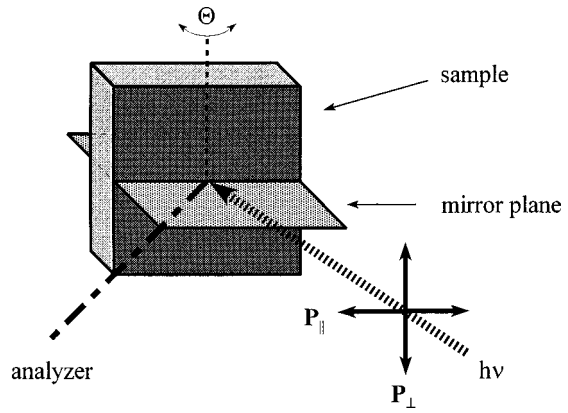

FIG. 2. A sketch of the experimental geometry. The incoming synchrotron radiation and the electron energy analyzer are situated in a mirror plane of the sample surface. The polarization vector of the radiation can lie either in ($\mathbf{P}\|$) or out of ($\mathbf{P}\perp$) the mirror plane. The magnitude of the wave vector is controlled via the polar angle Θ.

The experimental geometry is sketched in Fig. 2. The sample was oriented such that the incoming radiation and the photoelectron energy analyzer are situated in a mirror plane of the Cu_3O_4 plane. The polarization direction of the incident radiation could then be independently switched by using either the vertical or the horizontal undulator. In this manner additional information regarding the orbital symmetry of the initial states can be attained, as they can be classified as either even or odd with respect to reflection in the mirror plane.[11] When the polarization vector of the radiation lies in the mirror plane, excitation is only possible from initial states with even symmetry with respect to reflection in this plane. Alternatively, when the polarization vector is perpendicular to the incidence-emission plane, only excitation from initial states with odd symmetry is possible. The Cu_3O_4 plane of $Ba_2Cu_3O_4Cl_2$ contains two inequivalent structural mirror planes which can be used in such an experiment, which are labeled M_1 and M_2 in Fig. 1.

The band structure calculations were carried out in the local spin-density approximation plus on-site correlation (LSDA+U) using the linear combination of atomiclike orbitals (LCAO) method. For the LSDA, the parametrization of von Barth and Hedin was used and a scalar relativistic scheme with a minimum basis was applied. The states Cu ($4s$,$4p$,$3d$), O ($2s$,$2p$), Cl ($3s$,$3p$), and Ba ($6s$,$6p$,$5d$) have been taken as valence basis states, while the lower-lying states were treated as core levels. For taking into account the strong correlation at the copper sites, we applied a downward shift of the Cu $3d$ projected self-energy for all occupied band states with respect to an antiferromagnetic spin order of the Cu_A sublattice, and a ferromagnetic order of the Cu_B, which provides the correct translational symmetry for the Cu_B sublattice. As the photoemission experiment was carried out at temperatures well in excess of T_N^B, the Cu_B sublattice is in fact paramagnetic, with the local spin of the Cu $3d$ (Ref. 9) state fluctuating. This fluctuation is neglected in our treatment. The unoccupied minority spin Cu 3

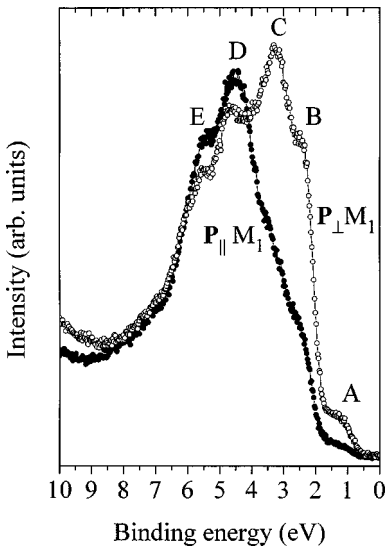

FIG. 3. Valence band photoemission spectra of $Ba_2Cu_3O_4Cl_2$ recorded at the Γ point with an angular resolution of $\pm 11°$. $\mathbf{P}\|M_1$: ●; $\mathbf{P}\perp M_1$: ○. The intensity is normalized at the Ba $5p_{3/2}$ peak at 13.8 eV binding energy (not shown).

d orbitals were shifted upwards in energy. The shift was adjusted such that the chemical potential is correctly located in the emerging charge transfer gap. For an assumed U of 8 eV, an upward shift of the unoccupied Cu $3d_{x^2-y^2}$ by 2 eV and a downward shift of the occupied, majority spin Cu $3d_{x^2-y^2}$ orbitals as well as both spin directions of the Cu $3d_{xy,xz,yz,3z^2-r^2}$ states by 6 eV resulted.[12] Using these shifts, the LSDA+U calculations were carried out self-consistently.

III. RESULTS AND DISCUSSION

In the following we will first present our polarization-dependent photoemission data of $Ba_2Cu_3O_4Cl_2$ followed by the results from the LSDA+U calculations. We then compare the photoemission and band structure data and discuss parallels with the CuO_2 plane system $Sr_2CuO_2Cl_2$ before summarizing.

A. Experimental results

The lattice constant in the Cu_3O_4 plane of $Ba_2Cu_3O_4Cl_2$ is 5.51 Å (Ref. 5), which, together with the plane geometry sketched in Fig. 1 gives a square two-dimensional (2D) Brillouin zone (BZ) of length ~ 0.57 Å^{-1}. The edge of the BZ is at 45° with respect to the Cu-O bonds. In order to ease comparison between the two oxychloride systems, we point out here that the Brillouin zone of $Ba_2Cu_3O_4Cl_2$ is rotated by 45° and has half of the area of that of $Sr_2CuO_2Cl_2$, with the result that the $(\pi,0)$ point of the Cu_3O_4 BZ coincides with the $(\pi/2,\pi/2)$ point of the CuO_2 BZ. Figure 3 shows photoemission spectra of the entire valence band, recorded with the polarization vector of the synchrotron radiation either perpendicular or parallel to the mirror plane M_1. These spectra were recorded at normal emission, with the angular acceptance of the electron energy analyzer set to $\pm 11°$, such that we average over a significant portion of the BZ, thus approximating a density of states (DOS) measurement. The valence band of $Ba_2Cu_3O_4Cl_2$ is approximately 6 eV wide

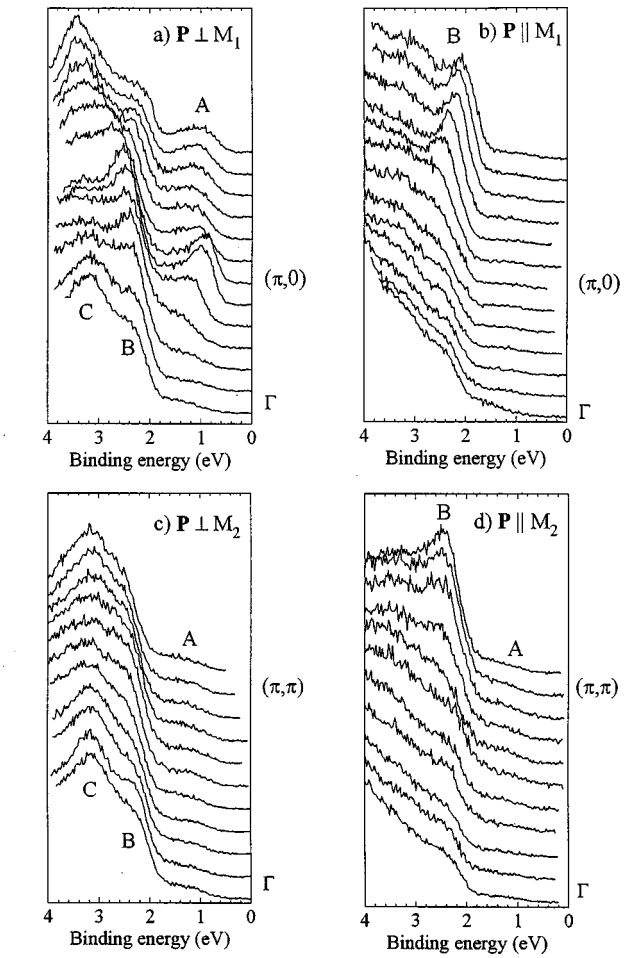

FIG. 4. Polarization-dependent ARPES spectra of $Ba_2Cu_3O_4Cl_2$ recorded along the two high symmetry directions. (a) $\Gamma\rightarrow(\pi,0)$, $\mathbf{P}\perp M_1$; (b) $\Gamma\rightarrow(\pi,0)$, $\mathbf{P}\|M_1$; (c) $\Gamma\rightarrow(\pi,\pi)$, $\mathbf{P}\perp M_2$; (d) $\Gamma\rightarrow(\pi,\pi)$, $\mathbf{P}\|M_2$.

and shows five features located at about 1.2 eV (A), 2.4 eV (B), 3.2 eV (C), 4.5 eV (D), and 5.5 eV (E) binding energy. Features A to C show considerable polarization-dependent intensity changes, whereby feature A loses the major part, and B and C about half of their intensity when the polarization vector lies in the mirror plane M_1.

In Fig. 4 angle-resolved spectra ($\Delta\theta=\pm 1°$) in a narrower binding energy range are presented. In panels (a) and (b) the wave vector is along the $\Gamma\rightarrow(\pi,0)$ direction of the BZ and the polarization vector of the exciting radiation is either perpendicular (a) or parallel (b) to the mirror plane M_1. For initial states of odd symmetry with respect to M_1 [Fig. 4(a)], we observe three features which have minimal binding energies of about 0.9 eV (A), 2.2 eV (B), and 3.2 eV (C). All features disperse by around 300 meV and show (in particular for peak A) strong **k**-dependent intensity modulation. For even initial states [Fig. 4(b)], only one feature (labeled B) is clearly visible as a peak and has a minimal BE of ~ 2.2 eV close to the $(2\pi,0)$ point and a dispersion of ~ 400 meV. This peak is superimposed upon a broad structure whose intensity reaches up into and beyond the binding energy region of feature C. We note that in Fig. 4(b) there is no signal corresponding to feature A. The significant intensity differences (for example, for feature B) between the spectra recorded at equivalent symmetry points (e.g., the Γ point in

the first and second BZ) indicates the strong **k** dependence of the photoemission matrix elements, which is a common feature in the cuprate high-temperature superconductors.

In panels (c) and (d) of Fig. 4 we present the corresponding spectra for the wave vector along the $\Gamma\rightarrow(\pi,\pi)$ direction. For initial states of odd symmetry with respect to M_2 [Fig. 4(c)], we observe two main features B and C. The former has a minimal BE of $\sim$2.2 eV at the Γ point and disperses upwards in BE by $\sim$300 meV on going from Γ to (π,π), while its intensity decreases. Feature C, located at $\sim$3.2 eV BE, shows no significant dispersion. There are signs of a weak, broad feature between 1–2 eV BE, which we label A. Although an accurate evaluation of the dispersion relation of feature A along $\Gamma\rightarrow(\pi,\pi)$ is difficult, a rough analysis shows that between the Γ point and (π,π) A disperses by maximally 150 meV, which is significantly less than that of the corresponding feature along the $\Gamma\rightarrow(\pi,0)$ direction [Fig. 4(a)]. For initial states of even symmetry with respect to M_2 [Fig. 4(d)], only a single clear feature labeled B is resolved as a peak at $\sim$2.2 eV near the (π,π) point. As in Fig. 4(b), this peak sits upon a broad background structure stretching beyond the measured binding energy range. There are also indications of a weak, broad feature at lower BE's, which we label A.

Before going further, it is instructive at this stage to discuss briefly the possible origin of the features observed in the photoemission data shown in Fig. 4. It is widely accepted that the first electron removal states in undoped cuprates are Zhang-Rice singlets (ZRS's).[13] Indeed, the singlet nature of these states has been verified for copper oxide (CuO).[14] Furthermore, the dispersion of the ZRS's formed by photoemission from the undoped CuO_2 and Cu_3O_4 plane oxychlorides $Sr_2CuO_2Cl_2$ and $Ba_2Cu_3O_4Cl_2$ has been studied recently using angle resolved photoemission.[8,15,16] In the case of $Ba_2Cu_3O_4Cl_2$, two possible ZRS's exist, located on either the Cu_A (ZRS_A) or Cu_B (ZRS_B) subsystems.[8] By comparison with model calculations, it could be shown that the dispersion relations of each of these ZRS's depends critically on the spin background of the respective subsystem, whereby ZRS_A experiences an antiferromagnetic[9] and ZRS_B an effectively paramagnetic spin background.[8] Consequently, the bandwidth of ZRS_A is proportional to the exchange integral between Cu_A sites J_A whereas the dispersion of ZRS_B is given by the effective hopping integral between Cu_B sites t_B. These two different ZRS's are the origin of the feature A observed at lowest binding energy in Fig. 4(a).

The dispersion relations of the three main features observed in the photoemission spectra (A, B, and C) are shown as symbols in Fig. 5. The majority of the data are from Figs. 4(a) and 4(c) (filled symbols), and represent measurements with the polarization vector perpendicular to the relevant mirror plane, whereas the open symbols are from Figs. 4(b) and 4(d) in which the polarization vector lies parallel to the incidence-emission plane. These data are the first measurements of the dispersion of the valence bands of $Ba_2Cu_3O_4Cl_2$ along $\Gamma\rightarrow(\pi,\pi)$. In order both to emphasize the symmetry of the measured dispersion relations around $(\pi,0)$ as well as to take advantage of the different matrix elements, the data in Fig. 5 are also shown from $(\pi,0)$ to the Γ point in the second BZ [labeled $(2\pi,0)$]. The dispersion of feature A between Γ and $(\pi,0)$ has already been discussed above and in Ref. 8. A

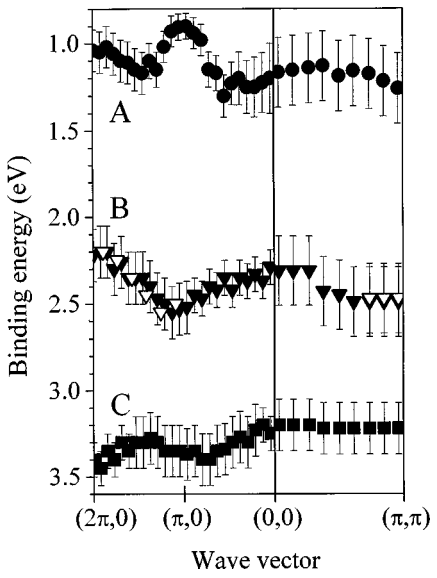

FIG. 5. Experimental dispersion relation of the main features in the photoemission spectra (labeled A, B, and C). Solid symbols represent measurements with the polarization vector perpendicular, and the open symbols parallel to the relevant mirror plane, respectively. The **k** range includes the Γ point in the second BZ in order to show the symmetry around the $(\pi,0)$ point.

straightforward interpretation of the features in the photoemission spectra along $\Gamma\rightarrow(\pi,\pi)$ is hampered by the fact that it is not possible to give every initial state a clear ''odd'' or ''even'' label with regard to its behavior on reflection in the mirror plane M_2. This is a consequence of the antiferromagnetic spin structure of the Cu_A subsystem which breaks the symmetry in M_2.[17] A way of envisaging this is to consider whether a translation parallel to the relevant mirror plane (simulating the splitting of the Cu_A sites into a spin-up and spin-down sublattice) and a reflection in the same mirror plane can be temporally exchanged or not. If they can, then all wave functions with a wave vector parallel to the mirror plane must be eigenfunctions of the reflection operator and can thus be classed as either symmetric or antisymmetric with respect to the mirror plane. This is the case for M_1, but not for M_2. Nevertheless, even for **k** along $\Gamma\rightarrow(\pi,\pi)$ the states which are *not* hybridized with Cu_A do maintain a clear symmetry.

In the remainder of this paper, however, we focus mainly on the valence band states at higher binding energies, such as features B and C in Fig. 4. These higher lying states in the CuO_2 plane oxychloride $Sr_2CuO_2Cl_2$ have recently been the subject of an ARPES study.[16] In this case, the next two features lying at higher BE than the ZRS were attributed to states which, at particular locations in **k** space [Γ, $(\pi,0)$, and (π,π)], possess practically *pure* O $2p$ character. For $Sr_2CuO_2Cl_2$ the first of these, located at 2.85 eV, has in-plane character, whereas the second feature at $\sim$4 eV should have out-of-plane character at Γ.[16] These nonmixing O states are essentially uncorrelated in nature and were suggested to be the origin of the so-called ''1 eV peak'' in the high-T_c cuprates, which had been discussed either in terms of an intrinsic feature of the electronic structure,[18] or in terms of a surface state.[19] It is of interest, then, to examine whether analogous oxygen states exist in the Cu_3O_4 plane of $Ba_2Cu_3O_4Cl_2$.

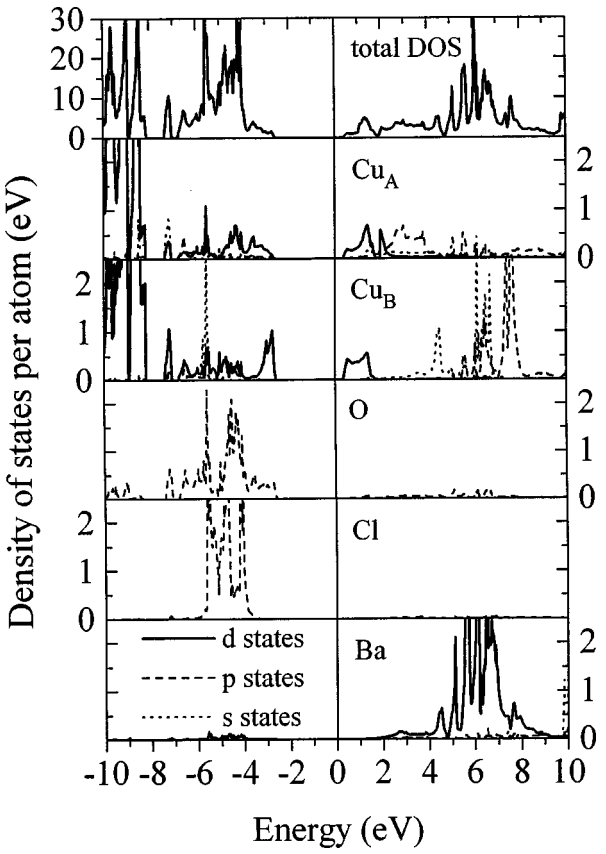

FIG. 6. Total and partial densities of states from the LSDA+U band structure calculation for $Ba_2Cu_3O_4Cl_2$, summed over both spin directions. The total DOS is given per cell, and the partial DOS per atom.

On inspection of the data in Fig. 4, it is clear that the features B and C are energetically not so distant from the nonmixing O states observed in $Sr_2CuO_2Cl_2$, and that under certain conditions, their intensity is maximal at the high symmetry points Γ, $(\pi,0)$, or (π,π). Given this initial similarity between the data from the two oxychloride systems, we have carried out calculations of the band structure of $Ba_2Cu_3O_4Cl_2$, in order to obtain a more detailed picture of the impact of the additional Cu_B on its electronic structure, and in particular in order to try to identify the bands giving rise to features B and C in the ARPES spectra.

B. Band structure calculations

The treatment of the quasiparticle band structure by LSDA+U as described above results in an insulating band structure for $Ba_2Cu_3O_4Cl_2$ in which an upper Hubbard band (UHB) appears and most of the occupied Cu 3d bands are shifted downwards in energy. The DOS resulting from the band structure as a sum of both spin directions is shown in Fig. 6. Also shown are the basis orbital projected DOS components [in the case of Cu_A we sum over the two Cu_A sites in the antiferromagnetic (AFM) unit cell]. The states below about 8 eV in the DOS would correspond to the $3d^8$ satellite observed at about 14 eV in the photoemission spectra of cuprates. The reasons for this discrepancy in energy are discussed, for example, in Ref. 20. As can be seen from a comparison of the DOS with the overview spectra shown in Fig. 3, the calculated valence band width of about 5 eV is in excellent agreement with experiment. Interestingly, in comparison to $Sr_2CuO_2Cl_2$, the Cl 3p states are calculated to lie at significantly lower BE in the barium oxychloride, but do not however have significant intensity for the photon energy used in the experiment.[21] Ba states only contribute significantly at higher binding energies. As in other cuprates, the partial DOS of $Ba_2Cu_3O_4Cl_2$ clearly shows the strong hybridization of Cu 3d and O 2p states in the valence band.

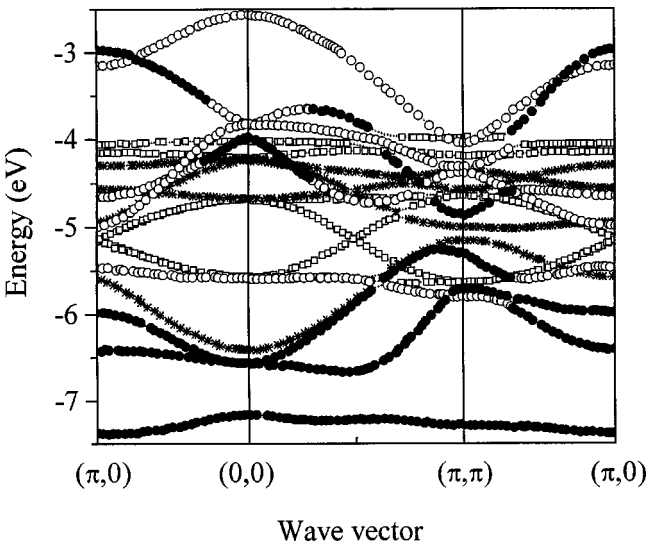

FIG. 7. LSDA+U band structure of $Ba_2Cu_3O_4Cl_2$ (small crosses) for one spin direction. Those bands with an identifiable orbital character are shown as symbols: ⋆ = bands from out-of-plane O $2p_z$ orbitals; □ = bands from Cl 3p orbitals; ● = bands involving predominantly σ combinations of O $2p_{x,y}$ orbitals; ○ = bands involving predominantly π combinations of O $2p_{x,y}$ orbitals.

The band structure itself for one spin direction is presented in Fig. 7 which includes a detailed analysis of the orbital character and the mirror symmetry (with respect to M_1 and M_2) of a number of the bands. These data can be compared with earlier LDA calculations,[22] both of which give a valence band composed of states resulting from hybridzation of Cu 3d, O 2p, and Cl 3p orbitals. However, the electron correlation makes itself felt in the LSDA+U case via the lowering in energy of the Cu 3d states. This means that the bands just below the chemical potential have a high degree of oxygen character. In addition, the LSDA+U calculation delivers a better agreement with the observed dispersion of the valence band features. There is a certain range of U (6 to 10 eV) for which the LSDA+U results for the first few eV below the chemical potential are insensitive to the precise value of U, and in the following we will discuss the case of $U=$ 8 eV as a representative example.

In order to help interpret the polarization dependences observed in experiment, it is important to understand the mirror symmetries of the calculated bands shown in Fig. 7. As mentioned earlier, the wave functions along $\Gamma\rightarrow(\pi,0)$ can be classed as either symmetric or antisymmetric with respect to M_1 and thus strictly can only be observed with the polarization vector of the exciting radiation either parallel or perpendicular to the incidence-emission (mirror) plane, respectively. Thus, all bands running along the $\Gamma\rightarrow(\pi,0)$ direction in Fig. 7 can be labeled as either S (symmetric) or A

TABLE I. A summary of the low-lying Cu and O-derived in-plane valence bands of $Ba_2Cu_3O_4Cl_2$ at the three high symmetry points Γ, $(\pi,0)$, and (π,π) from the LSDA+U band structure calculation for one spin direction. Shown are the energy in eV, the name of the band involved (see Fig. 8) and the respective weights for the orbitals or orbital sets O_σ, O_π, $Cu_A\ 3d_{x^2-y^2}$, $Cu_A\ 3d_{xy}$, $Cu_B\ 3d_{x^2-y^2}$, and $Cu_B\ 3d_{xy}$. In addition, the symmetry of each band with respect to the mirror planes M_1 and/or M_2 is shown: A=antisymmetric, S=symmetric, and M=mixed. The bands are listed in order of decreasing energy at each of the **k** points considered. The corresponding bands with in-plane O $2p_{x,y}$ character shown in Fig. 7 can be easily identified.

					Γ					
	Energy		O_σ	O_π	$Cu_A\ 3d_{x^2-y^2}$	$Cu_A\ 3d_{xy}$	$Cu_B\ 3d_{x^2-y^2}$	$Cu_B\ 3d_{xy}$	M_1	M_2
1	-2.568	π_1	0	0.994	0	0	0.165	0	A	S
2	-3.832	π_2	0.449	0.593	0	0	0	0	A	M
3	-3.832	$\tilde{\pi}_2$	0.226	0.593	0	0	0	0	S	M
4	-3.983	σ_1	0.548	0	0.460	0	0	0	A	A
5	-5.594	$\tilde{\pi}_1$	0	0.539	0	0.238	0	0	S	S
6	-6.568	σ_2	0.422	0.242	0	0	0	0	A	M
7	-6.568	$\tilde{\sigma}_2$	0.277	0.242	0	0	0	0	S	M
8	-7.162	$\tilde{\sigma}_1$	0.231	0	0	0.025	0	0.400	S	A
					$(\pi,0)$					
	Energy		0_σ	0_π	$Cu_A\ 3d_{x^2-y^2}$	$Cu_A\ 3d_{xy}$	$Cu_B\ 3d_{x^2-y^2}$	$Cu_B\ 3d_{xy}$	M_1	
1	-2.969	σ_2	0.514	0.270	0.143	0	0	0	A	
2	-3.148	π_1	0	0.844	0.025	0	0.177	0	A	
3	-4.650	π_2	0.191	0.606	0.065	0	0	0	A	
4	-4.990	$\tilde{\pi}_2$	0.051	0.649	0	0.080	0	0	S	
5	-5.465	$\tilde{\pi}_1$	0.117	0.494	0	0.107	0	0.011	S	
6	-5.982	σ_1	0.585	0.025	0.154	0	0.023	0	A	
7	-6.415	$\tilde{\sigma}_1$	0.284	0.057	0	0.052	0	0.253	S	
8	-7.379	$\tilde{\sigma}_2$	0.376	0.022	0	0.011	0	0	S	
					(π,π)					
	Energy		O_σ	O_π	$Cu_A\ 3d_{x^2-y^2}$	$Cu_A\ 3d_{xy}$	$Cu_B\ 3d_{x^2-y^2}$	$Cu_B\ 3d_{xy}$	M_2	
1	-4.050	π_1	0	0.732	0	0	0.229	0	S	
2	-4.315	π_2	0	0.824	0	0.102	0	0	M	
3	-4.385	$\tilde{\pi}_2$	0	0.831	0	0.081	0	0	M	
4	-4.865	$\tilde{\sigma}_1$	0.624	0	0	0	0	0.149	A	
5	-5.307	σ_2	0.362	0	0.252	0	0	0	M	
6	-5.719	σ_1	0.626	0	0	0	0	0	A	
7	-5.809	$\tilde{\pi}_1$	0	0.583	0	0	0	0	S	
8	-7.291	$\tilde{\sigma}_2$	0.431	0	0.084	0	0	0	M	

(antisymmetric) (see Table I for the assignment of the individual bands). In the $\Gamma\rightarrow(\pi,\pi)$ direction, for which M_2 is the relevant mirror plane, no such clear parity exists. Nevertheless, those bands which arise from the Cu_B subsystem retain a high degree of parity, as it is only Cu_A which breaks the M_2 reflection symmetry. Thus, for example, Cu_B $3d_{x^2-y^2}$ is even with respect to M_2 and Cu_B $3d_{xy}$ is odd. Consequently, the bands along $\Gamma\rightarrow(\pi,\pi)$ can be labeled as S (dominantly symmetric), A (dominantly antisymmetric), or M (of mixed symmetry, i.e., hybridizing mainly with the Cu_A subsystem).

The reflection symmetry of the individual bands was analyzed via their orbital character. In the energy region displayed in Fig. 7, we find bands with dominantly Cl $3p$ or O $2p$ character which have an admixture of Cu $3d$ character. We could identify six Cl $3p$ bands, two of which have predominantly Cl $3p_z$ character—the remaining four being composed primarily of Cl $3p_{x,y}$ orbitals. As discussed above, the low cross section for Cl $3p$ emission at the photon energy used here[21] means that the Cl $3p$-derived bands play little role in the experimental spectra.

The oxygen bands can be separated into two subgroups corresponding to out-of-plane O $2p_z$ and in-plane O $2p_{x,y}$ orbitals. Four bands in Fig. 7 arise from the former but, upon consideration of the experimental geometry sketched in Fig. 2, one would expect zero intensity for p_z states for the polarization vector of the synchrotron radiation oriented perpendicular to the incidence-emission plane [Figs. 4(a) and 4(c)], as the polarization vector is then orthogonal to the p_z orbitals. When the polarization vector of the radiation is aligned in the incidence-emission plane [Figs. 4(b) and 4(d)], emission from the p_z orbitals will be possible, but will be increasingly supressed at higher values of the polar angle θ as the sample is rotated away from normal emission in order

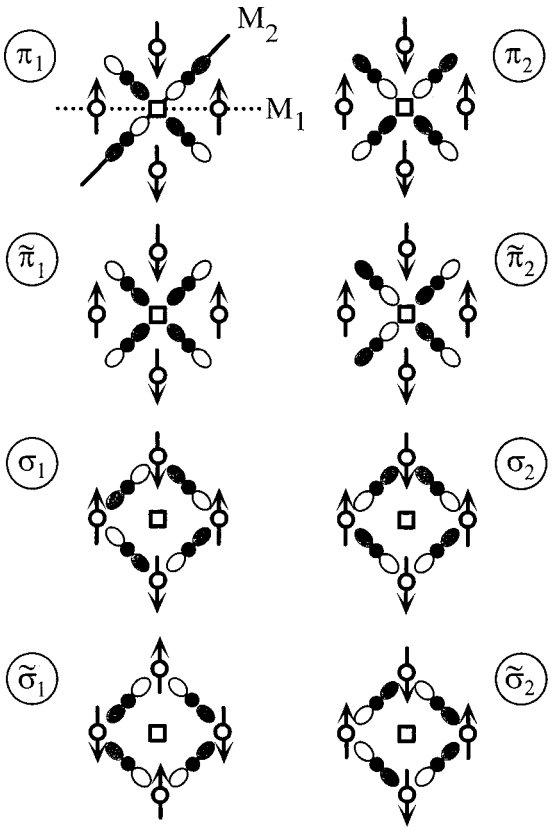

FIG. 8. Sketch of the different combinations of planar oxygen orbitals involved in the band structure. The shading indicates the sign of the orbital wave functions. ○ : Cu_A ; □ : Cu_B ; ● : oxygen. M_1 and M_2 are the two mirror planes parallel to the corresponding wave vectors $(\pi,0)$ and (π,π), respectively. The spin direction of the antiferromagnetically ordered Cu_A sublattice is schematically indicated by the arrows. Orbital combinations directed to Cu_A are denoted σ, and those directed to Cu_B are denoted π, whereby the presence or lack of a tilde denotes those which are symmetric or antisymmetric with respect to M_1, respectively.

to alter **k**. Consequently, in the discussion of the O $2p$-derived states below, we concentrate on those from the in-plane O $2p_{x,y}$ orbitals.

In order to discuss these bands, it is useful to introduce the notation shown in Fig. 8. Since there are four oxygen atoms in the unit cell of the Cu_3O_4 plane and two in-plane O $2p$ orbitals at each site, we have eight in-plane oxygen bands. In the following, the O $2p$ orbitals which point towards the Cu_A atoms are denoted as σ, and those pointing at right angles to Cu_A as π (see also, Ref. 23). These orbital sets can be further split between those which are symmetric ($\tilde{\pi}_1$, $\tilde{\pi}_2$, $\tilde{\sigma}_1$, and $\tilde{\sigma}_2$) or antisymmetric (π_1, π_2, σ_1, and σ_2) with respect to M_1. The orbital sets π_1, $\tilde{\pi}_1$, σ_1, and $\tilde{\sigma}_1$ have a defined parity with respect to M_2, the others do not. For our symmetry analysis of the in-plane O $2p$ bands, we calculated the corresponding orbital projections of all of these groups of states. At each of the high symmetry points it is possible to determine with which of the in-plane Cu $3d_{x^2-y^2}$ or $3d_{xy}$ orbitals the oxygen combinations shown in Fig. 8 can hybridize.[24] The corresponding weights are shown in Table I.

Thus following these procedures, we can determine both the orbital character of the in-plane oxygen bands at the high symmetry points, as well as their symmetry properties with respect to the mirror planes M_1 and M_2 as drawn in Fig. 8. We now work our way progressively through the band structure, starting at the states with lowest BE.

Only the π_1 combination hybridizes with the Cu_B $3d_{x^2-y^2}$ orbital, and forms the lowest BE band among all of the oxygen π bands. As the spin of the π_1 band is antiparallel to that of the Cu_B $3d_{x^2-y^2}$ UHB [which appears in the spin-down bandstructure above the Fermi level (not shown)], we conclude that the π_1 band represents the ZRS_B within our simple picture. Upon an improved treatment of the strong electron correlations (see, for example, our model calculation in Ref. 8), the ZRS_B bandwidth would be much smaller than that shown in Fig. 7. Nevertheless, the form of the dispersion should be conserved. In a similar way, one can also identify the ZRS_A. It has lowest BE at $(\pi,0)$ as the σ_2 spin-up oxygen band which hybridizes with the Cu_A $3d_{x^2-y^2}$ spin-down sublattice. Once again, the form of the dispersion shown here is in rough agreement with the model calculation,[8] but the bandwidth is strongly overestimated in the LSDA+U calculation. It should be noted that at the Γ point, a clear indication exists only for a ZRS_B singlet band. As can be seen from Fig. 7 and Table I at Γ there is no band at this energy with appreciable Cu_A character. This lends weight to the arguments put forward above that also along $\Gamma\rightarrow(\pi,\pi)$ feature A results from both ZRS_A and ZRS_B.

With increasing BE in Fig. 7 we then find at Γ a doubly degenerate band of pure oxygen character which is composed mainly of π_2 and $\tilde{\pi}_2$ orbitals with some admixture of σ_2 and $\tilde{\sigma}_2$. A little below these states at Γ, there is a third oxygen band (σ_1), which is antisymmetric with respect to both M_1 and M_2. These three oxygen bands together comprise the edge of the main valence band at Γ. Along $\Gamma\rightarrow(\pi,0)$, the valence band edge is built up of two nonbonding oxygen bands: one is symmetric ($\tilde{\pi}_2$) and the other is antisymmetric [σ_1, going over to a π_2 band at $(\pi,0)$]. Both bands intersect along this line in **k** space such that the antisymmetric band has smaller BE at $(\pi,0)$. Along $\Gamma\rightarrow(\pi,\pi)$, the valence band edge is composed of the π_2 band, which has mixed character.

Next in binding energy comes the nearly dispersionless $\tilde{\pi}_1$ band which, at least along $\Gamma\rightarrow(\pi,0)$ has symmetric character with respect to the incidence-emission plane. At $(\pi,0)$ for still higher BE's lies a second band σ_1 which derives from the hybridization of a σ orbital combination with Cu_A (the first being the ZRS_A). A detailed inspection shows that at $(\pi,0)$, the σ_1 orbital combination hybridzes with the Cu_A $3d_{x^2-y^2}$ orbitals, but in contrast to the σ_2 (ZRS_A) band discussed above, with the spin-up Cu_A sublattice. This entity then possesses parallel oxygen and copper spins and therefore we can interpret the σ_1 band around $(\pi,0)$ as a spin triplet state of the Cu_A subsystem.

C. Comparison of experiment with the calculated bands

We deal here first with the dispersion of feature A along $\Gamma\rightarrow(\pi,\pi)$, and argue that this weak feature corresponds to a combination of ZRS_A and ZRS_B, whereby the relatively large errors in the determination of its energy make the experimental distinction between the two Zhang-Rice singlets

impossible. As a consequence of the even symmetry of the Cu_B $3d_{x^2-y^2}$ orbital with respect to M_2 we expect to observe the ZRS_B for the polarization vector of the synchrotron radiation parallel to M_2. This then corresponds to feature A in Fig. 4(d). However, the ZRS_A has no clear parity for **k** along $\Gamma\rightarrow(\pi,\pi)$, and should therefore be visible for both $\mathbf{P}\|M_2$ and $\mathbf{P}\perp M_2$. Indeed, a weak feature A is certainly visible for the polarization vector perpendicular to M_2 in Fig. 4(c). The relatively flat dispersion of the ZRS between Γ and (π,π), at least in comparison to that along $\Gamma\rightarrow(\pi,0)$ observed in Figs. 4 and 5 is also in agreement with the predictions for the dispersion of a single hole in a CuO_2 plane from the *t-J* model, which is more successful in treating the strong electron correlation present in these cuprates.[1,25]

In the following we compare the experimental photoemission spectra in the energy regions of features B and C with the calculated LSDA+*U* bands. The situation for **k** along $\Gamma\rightarrow(\pi,0)$ with polarization perpendicular to the mirror plane [Fig. 4(a)] is the most clear. In this geometry the p_z states do not contribute to the spectra and thus in the experiment we measure mainly the planar oxygen-derived bands which are antisymmetric with respect to M_1. As can be seen from Fig. 7 and Table I, apart from the ZRS's, there are two further bands with the correct symmetry between Γ and $(\pi,0)$, which in the notation of Fig. 8 are labeled π_2 and σ_1 at the high symmetry point $(\pi,0)$. The agreement with experiment here is good insofar as Fig. 4(a) contains three clear features A, B, and C which would then correspond to the ZRS bands (π_1 and σ_2), and the oxygen bands π_2 and σ_1, respectively. In addition, the fact that the antisymmetric band π_2 swaps in energy with the symmetric $\tilde{\pi}_2$ band, such that the former lies at lowest BE at $(\pi,0)$, is consistent with the observation that at $(\pi,0)$ a significant part of the peak intensity of feature B is only observed for $\mathbf{P}\perp M_1$. In the energy region corresponding to feature B, the calculation also predicts only a single symmetric band with respect to M_1 between Γ and $(\pi,0)$ (labeled $\tilde{\pi}_2$), which is also consistent with the single edgelike structure observed in Fig. 4(b). As mentioned above, at $(\pi,0)$ σ_1 is the spin triplet band of Cu_A, which thus gives an experimental singlet-triplet splitting of around 2.5 eV. This is slightly less than the value of 3 eV arrived at in the LSDA+*U* calculation. Calculations for a CuO_4 cluster give an energy separation of 1.5 and 3.4 eV between the $^1A_1$ (ZR) singlet and the $^3B_1$ and $^3A_1$ triplet states, respectively.[26] The spin triplet band of the Cu_B system is seen in our calculation only in the band structure of the spin direction not shown in Fig. 7 (the band structure is ferromagnetically split with respect to Cu_B). It lies in between the nonbonding π_2 orbital combination and the Cu_A spin triplet σ_1 seen in Fig. 7 at $(\pi,0)$.

Due to the lack of pure parity for some bands with respect to reflection in M_2, the data along $\Gamma\rightarrow(\pi,\pi)$ are more difficult to interpret. This situation is further complicated for $\mathbf{P}\|M_2$ by the additional presence of emission from the bands derived from O $2p_z$ orbitals. Nevertheless, one contact point between the calculation and experiment is the predicted reduced bandwidth along Γ to (π,π) in comparison to that along Γ to $(\pi,0)$, whereby in the experiment practically no dispersion is observed along (π,π). Furthermore, the mixed symmetry character along $\Gamma\rightarrow(\pi,\pi)$ predicted in the LSDA+*U* calculation is borne out in the presence of spectral structures for both orientations of the polarization vector of the synchrotron radiation.

An attempt to make a more quantitative comparison between the experimental dispersion relations such as those shown in Fig. 5 and the results of the LDA+*U* calculation is of limited value, as the electron correlation effects have been taken into account via a relatively crude procedure in terms of a single parameter *U* in a mean field manner. The inclusion of additional correlation terms (such as U_{pp} or U_{pd}, for instance) would be expected to lead to a better quantitative agreement between theory and experiment. However, such refinements are beyond the scope of this paper which aims to provide an initial analysis of the rather complex valence band structure of $Ba_2Cu_3O_4Cl_2$, utilizing the ability of the LSDA+*U* calculations to accurately predict the character and symmetry of the electronic states in question.

It is evident from the discussion above that the band structure within the first few eV of the chemical potential in $Ba_2Cu_3O_4Cl_2$ is considerably more complex than that of the CuO_2 plane oxychloride $Sr_2CuO_2Cl_2$. In particular, it is clear from Fig. 8 that the set of O $2p$ orbitals which are free to form the nonmixing O $2p$ states at (π,π) in $Sr_2CuO_2Cl_2$ (Ref. 16) are otherwise occupied in the Ba oxychloride: these correspond to the π_1 orbitals shown in Fig. 8 which form, together with the Cu_B $3d_{x^2-y^2}$, the basis for the ZRS_B.

The impact of Cu_B has also been observed on the low lying unoccupied electronic states in a comparative x-ray absorption study of $Sr_2CuO_2Cl_2$ and $Ba_2Cu_3O_4Cl_2$.[27] In this case, the upper Hubbard band feature seen in the O *K* absorption spectrum of $Ba_2Cu_3O_4Cl_2$ is both broader and more intense than that in the CuO_2 plane oxychloride, which is a result of the presence of two UHB's in the Cu_3O_4 plane material corresponding to the two copper subsystems. In addition, the higher lying unoccupied states are also affected by this, in that the hybridization between the in-plane O $2p_{x,y}$ and Cu_B $3d_{x^2-y^2}$ orbitals which gives rise to the UHB_B deprives the Ba $5d$ levels of hybridization partners. This leads to a reduced spectral weight for planar O $2p$ states above the UHB in $Ba_2Cu_3O_4Cl_2$, whereas in $Sr_2CuO_2Cl_2$ the in-plane and out-of-plane spectra above the UHB are essentially equivalent.[27]

Thus, we are able to develop a detailed picture of the impact of the altered Cu-O plane geometry and stoichiometry on the electronic states of a cuprate plane.

(i) The lowest lying electron removal states in both the CuO_2 and Cu_3O_4 plane materials are Zhang-Rice singlets. This follows, at least in part, from the identical local geometry of the CuO_4 plaquettes which form the building blocks of both Cu-O planes.

(ii) Each of the two copper subsystems in the Cu_3O_4 plane gives rise to a different Zhang-Rice singlet in photoemission[8] and a different upper Hubbard band.[27] The dispersion relation and symmetry of the ZRS from the Cu_AO_2 subsystem of $Ba_2Cu_3O_4Cl_2$ is very similar to that of a single hole in a normal antiferromagnetic CuO_2 plane, whereas the dispersion of ZRS_B reflects the lack of spin order on the Cu_B subsystem, and thus scales with the hopping integral between Cu_B sites t_B.

(iii) The electronic states further away from the chemical potential are also affected by the presence of Cu_B. In particular, the Cu_B offers the surrounding O $2p$ orbitals an additional hybridization partner. This results in significant differences in the occupied nonbonding oxygen-derived states between $Ba_2Cu_3O_4Cl_2$ and $Sr_2CuO_2Cl_2$, as well as in the anisotropy of the unoccupied electronic states above the UHB's of the two oxychlorides.

IV. CONCLUSIONS

We have presented a detailed joint experimental and theoretical investigation of the valence band electronic structure of the model cuprate $Ba_2Cu_3O_4Cl_2$. This oxychloride system possesses a Cu_3O_4 plane which can be regarded as a superposition of two copper subsystems: a ''normal'' Cu_AO_2 cuprate plane and an extra, magnetically frustrated Cu_B site. Thus $Ba_2Cu_3O_4Cl_2$ represents an ideal trial system for assessing the impact of deviations from the CuO_2 plane stoichiometry upon the electronic structure in cuprate materials.

From polarization-dependent, **k**-resolved photoemission measurements we have determined the dispersion relations and symmetry of the different valence bands. The experimental data have been compared with the results of band structure calculations carried out within the LSDA+U formalism, which included a detailed analysis of the character and symmetry of the individual bands involved. The calculated overall bandwidth agrees well with that observed in experiment, as does the hybridized O $2p$/Cu $3d$ nature of the majority of the valence band states.

The lowest lying electron removal states observed in the photoemission spectra represent Zhang-Rice singlets formed on the two sublattices within the Cu_3O_4 plane. Their dispersion relation is intimately linked to the spin background prevalent in each of the Cu subsystems (antiferromagnetic for Cu_A; paramagnetic for Cu_B), and can be well reproduced in model calculations.[8] While the bandwidth of these strongly correlated states is (not unexpectedly) poorly described in the LSDA+U calculation, the form of their dispersion relations, their symmetry characteristics, and their spin-singlet nature are all evident in the mean field calculation. The comparison of the photoemission data with the results of the LSDA+U calculation allows the determination of the identity of the deeper-lying valence bands. For example, along $\Gamma\rightarrow(\pi,0)$ the three structures observed in experiment for $\mathbf{P}\perp M_1$ correspond to the ZRS bands (π_1 and σ_2) and the oxygen bands π_2 and σ_1. The observed polarization-dependence of these features is also consistent with this assignment. In general, the states making up the main valence band edge at $\sim$2 eV binding energy could be shown to be mainly due to states involving in-plane combinations of O $2p_{x,y}$ orbitals, some of which exhibit essentially pure O $2p$ character.

However, the particular O $2p$ orbital combinations responsible for the most striking of the nonmixing oxygen states at (π,π) in $Sr_2CuO_2Cl_2$ are occupied in the formation of the ZRS on the Cu_B sublattice in $Ba_2Cu_3O_4Cl_2$. The deeper lying valence bands in $Ba_2Cu_3O_4Cl_2$ generally involve more hybridization with the Cu $3d$ levels than those nearer the chemical potential, and include a state observed some 3 (2.5) eV below the ZRS state in the calculation (experiment), in which the spin of the O $2p_{x,y}$ and Cu $3d_{x^2-y^2}$ states are parallel (spin triplet). Thus, despite the shortcomings inherent in the theoretical mean-field treatment of a correlated electron system, we show that in particular the combination of the experimental and theoretical data allow the development of a comprehensive picture of the impact of the extra copper site on the electronic structure of a CuO_2 plane.

ACKNOWLEDGMENTS

This work was partly funded by the BMBF (05-605BDA) and the Fonds der chemischen Industrie (G.K.). M.S.G. gratefully acknowledges the HCM program of the EU (ERBCHB1CT941136) and S.H. and H.R. are grateful to the Graduiertenkolleg der TU Dresden (DFG) for financial support. We thank V. Yu. Yushankhai and S.-L. Drechsler for fruitful discussions and W. Höppner for technical assistance.

[1] E. Dagotto, Rev. Mod. Phys. **66**, 763 (1994).

[2] J. Fink, N. Nücker, E. Pellegrin, H. Romberg, M. Alexander, and M. Knupfer, J. Electron Spectrosc. Relat. Phenom. **66**, 395 (1994).

[3] Z.-X. Shen and D. S. Dessau, Phys. Rep. **253**, 1 (1995).

[4] M. Greven, R. J. Birgeneau, Y. Endoh, M. A. Kastner, B. Keimer, M. Matsuda, G. Shirane, and T. R. Thurston, Phys. Rev. Lett. **72**, 1096 (1994).

[5] R. Kipka and Hk. Müller-Buschbaum, Z. Anorg. Allg. Chem. **419**, 58 (1976).

[6] F. C. Chou, A. Aharony, R. J. Birgeneau, O. Entin-Wohlman, M. Greven, A. B. Harris, M. A. Kastner, Y. J. Kim, D. S. Kleinberg, Y. S. Lee, and Q. Zhu, Phys. Rev. Lett. **78**, 535 (1997).

[7] K. Yamada, N. Suzuki, and J. Akimitsu, Physica B **213&214**, 191 (1995).

[8] M. S. Golden, H. C. Schmelz, M. Knupfer, S. Haffner, G. Krabbes, J. Fink, V. Yu. Yushankhai, H. Rosner, R. Hayn, A. Müller, and G. Reichardt, Phys. Rev. Lett. **78**, 4107 (1997).

[9] As discussed in Ref. 8, the magnetic correlation length on the Cu_AO_2 sublattice is such that at 360 K (30 K above T_N^A), at least as far as photoemission is concerned, this subsystem nevertheless represents an antiferromagnetically spin background.

[10] W. B. Peatmann, J. Bahrdt, F. Eggenstein, G. Reichardt, and F. Senf, Rev. Sci. Instrum. **66**, 2801 (1995).

[11] For example, A. Zangwill, *Physics at Surfaces* (Cambridge University Press, Cambridge, United Kingdom, 1988).

[12] V. I. Anisimov, J. Zaanen, and O. K. Andersen, Phys. Rev. B **44**, 943 (1991).

[13] F. C. Zhang and T. M. Rice, Phys. Rev. B **37**, 3759 (1988).

[14] L. H. Tjeng, B. Sinkovic, N. B. Brookes, J. B. Goedkoop, R. Hesper, E. Pellegrin, F. M. F. de Groot, S. Altieri, S. L. Hulbert, E. Shekel, and G. A. Sawatsky, Phys. Rev. Lett. **78**, 1126 (1997).

[15] B. O. Wells, Z.-X. Shen, A. Matsuura, D. M. King, M. A. Kastner, M. Greven, and R. J. Birgeneau, Phys. Rev. Lett. **74**, 964 (1995).

[16] J. J. M. Pothuizen, R. Eder, N. T. Hien, M. Matoba, A. A. Menovsky, and G. A. Sawatsky, Phys. Rev. Lett. **78**, 717 (1997).
[17] M_2 would once again be a true mirror plane for the $\Gamma \rightarrow (\pi, \pi)$ direction and the states would regain their pure symmetric or antisymmetric parity for Cu_A in a paramagnetic spin state. This would, however, yield a metallic ground state in the calculation, which is far from the experimental situation.
[18] For example, C. G. Olson, J. G. Tobin, G. D. Waddill, D. W. Lynch, and J. Z. Liu, J. Phys. Chem. Solids **56**, 1879 (1995).
[19] R. Claessen, G. Mante, A. Huss, R. Manzke, M. Skibowski, Th. Wolf, and J. Fink, Phys. Rev. B **44**, 2399 (1991).
[20] H. Eskes and G. A. Sawatsky, Phys. Rev. B **43**, 119 (1991).
[21] At 35 eV, the calculated respective relative atomic photoionization cross sections are (Mb) Cu $3d = 9.4$; O $2p = 8.0$; Ba $5p = 3.5$; and Cl $3p = 0.7$. J.-J. Yeh and I. Lindau, At. Data Nucl. Data Tables **32**, 1 (1985).
[22] H. Rosner and R. Hayn, Physica B **230-232**, 889 (1997).
[23] L. F. Mattheiss and D. R. Hamann, Phys. Rev. B **40**, 2217 (1989).
[24] In order to unambiguously determine the hybridization partners of the oxygen orbital combinations shown in Fig. 8, one needs to consider four unit cells. For the sake of simplicity, however, we have limited ourselves to a single cell in each case in the figure.
[25] V. Yu. Yushankhai, V. S. Oudovenko, and R. Hayn, Phys. Rev. B **55**, 15 562 (1997).
[26] H. Eskes, L. H. Tjeng, and G. A. Sawatzky, Phys. Rev. B **41**, 288 (1990).
[27] S. Haffner, R. Neudert, M. Kielwein, M. Knupfer, M. S. Golden, K. Ruck, G. Krabbes, J. Fink, H. Rosner, R. Hayn, H. Eisaki, S. Uchida, Z. Hu, M. Domke, and G. Kaindl, Phys. Rev. B **57**, 3672 (1998).